Desroches, M. F., Krauskopf, B., & Osinga, H. M. (2007). Mixed-mode oscillations and slow manifolds in the self-coupled FitzHugh Nagumo system.

Early version, also known as pre-print

Link to publication record in Explore Bristol Research
PDF-document

University of Bristol - Explore Bristol Research
General rights

Mixed-mode oscillations and slow manifolds in the self-coupled FitzHugh Nagumo system

Mathieu Desroches,* Bernd Krauskopf, and Hinke M. Osinga

Bristol Centre for Applied Nonlinear Mathematics,
Department of Engineering Mathematics, University of Bristol,
Queen's Building, Bristol BS8 1TR, United Kingdom
(Dated: August 8, 2007)

We investigate the organisation of mixed-mode oscillations in the self-coupled FitzHugh Nagumo system. This type of oscillations can be explained as a combination of relaxation oscillations and small-amplitude oscillations controlled by canard solutions that are associated with a folded singularity on a critical manifold. The self-coupled FitzHugh Nagumo system has a cubic critical manifold for a range of parameters, and an associated folded singularity of node type. Hence, there exist corresponding attracting and repelling slow manifolds that intersect in canard solutions. We present a general technique for the computation of two-dimensional slow manifolds (smooth surfaces). It is based on a boundary value problem approach where the manifolds are computed as one-parameter families of orbit segments. Visualisation of the computed surfaces gives unprecedented insight into the geometry of the system. In particular, our techniques allow us to identify canard solutions as the intersection curves of the attracting and repelling slow manifolds.

A mixed-mode oscillation (MMO) is an oscillatory cycle formed by several small-amplitude oscillations followed by a number of large excursions. While frequently observed in both experiments and models of chemical or biological systems [1], the precise mechanism that generates such MMOs in slow-fast systems has only recently been explained [2–4]. The main ingredients for the occurrence of MMOs are the presence of (at least) one fast variable, two slow variables and a folded critical manifold. The dynamics in such a system consists of slow motion on an attracting slow manifold, followed by a fast jump to another attracting slow manifold. This classical behaviour of a relaxation oscillation accounts for the large excursions of an MMO. The small-amplitude oscillations of the MMO, on the other hand, are organised by so-called canard solutions, which are intersection curves of attracting and repelling slow manifolds. In this paper we showcase a technique to compute attracting and repelling slow manifolds. Specifically, we explain how each slow manifold can be approximated as the one-parameter solution family of a two-point boundary value problem. By concatenation of two such boundary value problems we are able to identify the canard solutions that separate the slow manifolds into regions of different types of MMOs. We demonstrate our method by computing slow manifolds and canard solutions in the self-coupled FitzHugh Nagumo system — a model that arises in the study of synchronization in a network of neurons.

---

*Electronic address: M.Desroches@bristol.ac.uk

Throughout, we consider the self-coupled FitzHugh Nagumo system in the form

$$\begin{cases} v' = h - \dfrac{v^3 - v + 1}{2} - \gamma s v, \\ h' = -\varepsilon(2h + 2.6v), \\ s' = \beta H(v)(1 - s) - \varepsilon \delta s. \end{cases} \quad (1)$$

System (1) is a simplified model for the study of synchronization in a network of Hodgkin-Huxley neurons; see also Wechselberger [4]. In particular, this model represents only one neuron with self-coupling, which is equivalent to a network of coupled neurons. The variable v represents the voltage potential of the neuron membrane, h the inactivation of the sodium channels, and s the synaptic coupling in the network. The parameter γ is the coupling strength, β the activation rate, and ε and δ determine the decay rates of inactivation h and the synapse s. By means of the Heaviside function $H(v)$, system (1) incorporates the feature that s varies slowly when $v < 0$ (the silent phase), while s is fast when $v > 0$ (the active phase). Note that the parameter β only plays a role when the system is in the active phase. Indeed, ε acts as the singular perturbation parameter and both h and the deactivation of s evolve on a much slower timescale than the voltage potential v.

If the self-coupling is not present ($\gamma = 0$) then the neuron fires an action potential at a rate of about 100 Hz. The introduction of the synaptic coupling with a particular strength $\gamma > 0$ substantially slows down the firing rate, and small-amplitude oscillations can be observed in between the action potentials; see already Fig. 1(a) where the frequency of the action potentials is only about 5 Hz.

The self-coupled FitzHugh Nagumo system was used by Wechselberger [4] to illustrate how canards organise the behaviour in a real application. His analysis focused on how the canard solutions divide the attracting slow manifold into sectors that correspond to an increasing

number of small-amplitude oscillations. We take this analysis further by computing the actual attracting and repelling slow manifolds. While similar in spirit to the work of Wechselberger [4] and Milik *et al.* [2], our computational technique is based on the continuation of two-point boundary value problems [5], which is more powerful and versatile than integration methods used previously. Furthermore, within our set-up we can calculate the canard solutions directly as the intersection of an attracting and a repelling slow manifold. This offers the possibility of following canard solutions when a parameter of the system is varied. The method presented here has been used in [6] to compute slow manifolds and associated canard solutions for a three-dimensional normal form of a slow-fast system with a folded node; we refer to [4, 7] for details on different normal forms of the folded node singularity. In the normal-form setting a start solution for the computation is known analytically. The self-coupled FitzHugh Nagumo system studied here also has a folded node, but it is not in normal form and no start solution is known. The aim of this paper is to show how one can compute the slow manifold in this more general application setting.

This paper is organised as follows. In the next section we present relevant properties of (1) in the silent phase in between the action potentials, where we closely follow [4]. Section II explains how a two-point boundary value problem can be set up for the computation of the attracting and repelling slow manifolds. We also discuss how the concatenation of two such boundary value problems can be used for finding canard solutions. We end with a discussion in Sec. III.

I. PROPERTIES OF THE SELF-COUPLED FITZHUGH NAGUMO SYSTEM

The occurrence of MMOs in the self-coupled FitzHugh Nagumo system is organised by the dynamics of the silent phase in between the action potentials. This phase can be defined as $v < 0$; compare also Fig. 1(a). For $v < 0$ the Heaviside function $H(v) \equiv 0$ in system (1), so that we only need to study the silent-phase system

$$
\begin{cases}
v' = h - \dfrac{v^3 - v + 1}{2} - \gamma s v, \\
h' = -\varepsilon(2h + 2.6v), \\
s' = -\varepsilon \delta s.
\end{cases}
\tag{2}
$$

We consider the self-coupled FitzHugh Nagumo system (1) for the fixed silent-phase system (2) given by $\gamma = 0.5$, $\varepsilon = 0.015$ and $\delta = 0.565$. The dynamics of (2) gives rise to MMOs of (1) (that also involve the active phase where $v > 0$).

System (2) has the natural formulation of a three-dimensional slow-fast system with two slow variables h and s and one fast variable v. There is a wealth of literature on the dynamics of slow-fast systems of this type;

we refer to [8–18] for an entry into the literature. An important object is the critical manifold S for $\varepsilon = 0$, which for a three-dimensional system with two slow variables is a surface. For system (2), the critical manifold S is implicitly defined by the equation $v' = f(v, h, s) = 0$, which gives

$$
S := \left\{ (v, h, s) \in \mathbb{R}^3 \;\middle|\; h = \frac{v^3 + (2\gamma s - 1)v + 1}{2} \right\}.
\tag{3}
$$

The surface S has a fold (with respect to the fast variable v) along the curve

$$
F := \left\{ (v, h, s) \in \mathbb{R}^3 \;\middle|\; h = \frac{1}{2} - v^3, \; s = \frac{1 - 3v^2}{2\gamma} \right\}.
\tag{4}
$$

The fold curve F has a cusp point at $(v, h, s) = (0, \frac{1}{2}, \frac{1}{2\gamma})$ and divides the surface S into an attracting and a repelling sheet. For suitable γ the critical manifold S is folded in the physically realistic range $s \in [0, 1]$ and consists there locally of two attracting and one repelling sheets. (Note that one of the attracting sheets lies outside the region of interest, namely, it exists for $v > 0$.)

The critical manifold S is normally hyperbolic everywhere except in the vicinity of the fold curve F. So according to Fenichel theory [19], away from F the attracting and repelling sheets of S perturb smoothly to invariant attracting and repelling manifolds for $\varepsilon > 0$, respectively. This means that system (2) also has attracting and repelling slow manifolds in the range $s \in [0, 1]$. The dynamics for small ε is therefore as follows. A trajectory generated by system (2) that starts at an arbitrary point on the (admissible) attracting sheet of S will follow this sheet until it reaches F. At F the trajectory may jump, that is, it leaves S; the trajectory will then leave the admissible space $v < 0$, so that the further dynamics is dictated by system (1). However, the trajectory may actually cross the fold curve and continue for some time near the repelling sheet of S; such a trajectory is called a canard solution.

In order to study this behaviour, it is customary to determine the so-called desingularised reduced system of system (2). Rather than expressing the slow flow in terms of the slow variables h and s, we consider the flow in terms of v and s and think of h as a function of v and s. A rescaling of time with the factor $-\frac{\partial}{\partial v} f(v, h, s)$ leads to the desingularised reduced system

$$
\begin{cases}
\dot{v} = -v^3 + 1.6v - (2 + \delta)\gamma s v - 1, \\
\dot{s} = -\delta s \dfrac{3v^2 - 1 + 2\gamma s}{2}.
\end{cases}
\tag{5}
$$

The dynamics of (5) determines the dynamics on S; we can project the phase portrait of system (5) onto S, but then time must be reversed on the repelling sheet of S where $\frac{\partial}{\partial v} f(v, h, s) > 0$. In particular, an equilibrium of system (5) that lies on the fold curve F is called a *folded singularity*, but note that a folded singularity is not an equilibrium of the flow on S. For all $\delta > 0$ system (5)
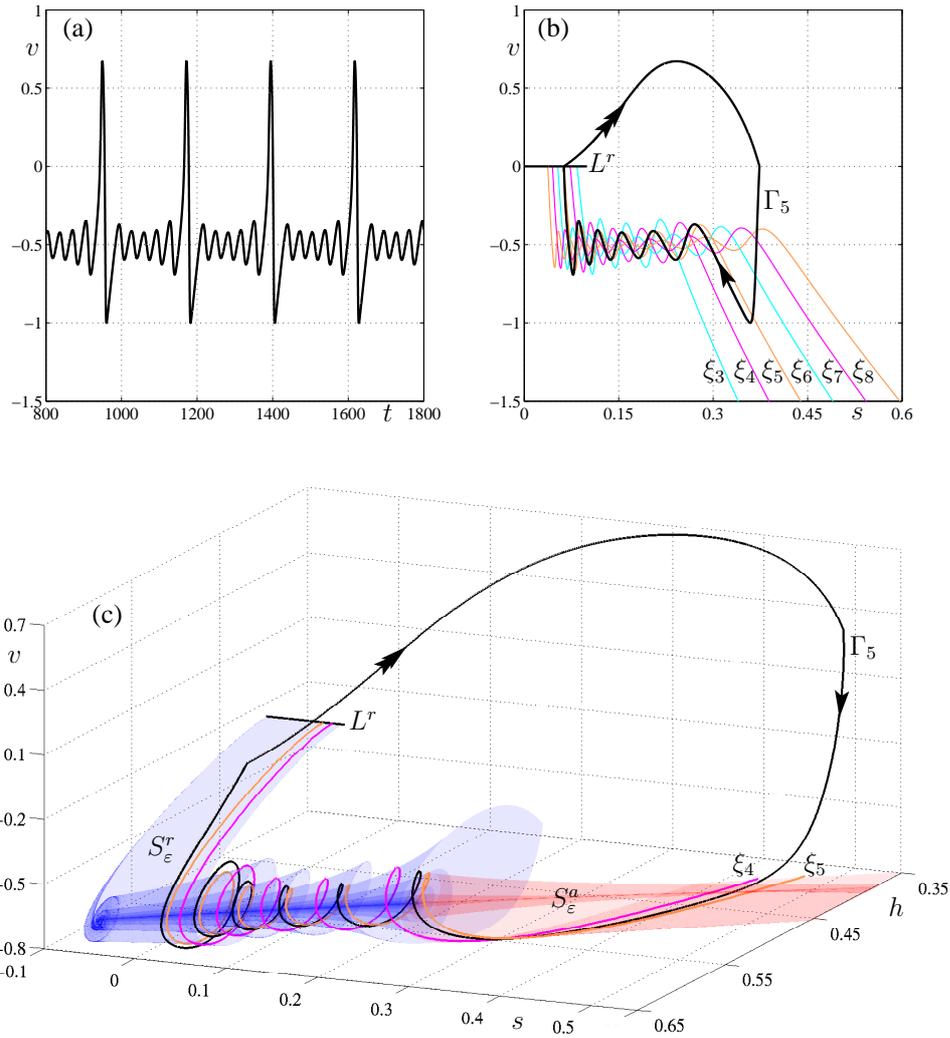
FIG. 1: The geometry of the MMO of system (1) for $\beta = 0.035$, where $\gamma = 0.5$, $\varepsilon = 0.015$, and $\delta = 0.565$. Panel (a) shows its time evolution of the voltage potential v. Panel (b) shows the MMO periodic orbit Γ_5 projected onto the (h,v)-plane, together with six canard solutions (labelled ξ_3–ξ_8) of the silent-phase system (2). Panel (c) shows Γ_5 with the associated attracting slow manifold S_ε^a (red surface) and repelling slow manifold S_ε^r (blue surface) of (2), both calculated up to a plane through the folded node; also shown are the two neighboring canard solutions ξ_4 and ξ_5.

has a folded node $\mathbf{p}_{\text{fn}}$ on F with $v < 0$; for our choice of parameters $\mathbf{p}_{\text{fn}} \approx (-0.4900, 0.6176, 0.2797)$. As a result there are trajectories on the attracting sheet of S that converge to the folded node in finite time and then pass through it with nonzero speed (hence following the repelling sheet of S for some time); these trajectories are called *singular canards* [8].

The folded node $\mathbf{p}_{\text{fn}}$ on S and the corresponding singular canard solutions generate actual canard solutions for system (2), which in turn generate MMOs for the self-coupled FitzHugh Nagumo system (1). Figure 1 gives an idea of what this looks like for a particular choice of parameters. Panel (a) shows the time evolution of the voltage v of the MMO of system (1) for $\beta = 0.035$. In this case there are five small-amplitude oscillations in between

each large spike of the action potential, which means that the MMO is of type 1^5 [20]. Figure 1(b) shows a projection of the MMO periodic orbit Γ_5 onto the (h,v)-plane. Also shown are projections of some of the canards (labelled ξ_3 to ξ_8) of system (2). Fig. 1(c) shows the three-dimensional view of Γ_5 with the attracting (denoted S_ε^a) and repelling (denoted S_ε^r) slow manifolds; here only the canards ξ_4 and ξ_5 are shown. Notice how the canards rotate around the fold curve F; the number of rotations is represented in their labelling.

Figure 1 shows that the silent phase of the MMO is organised by the canards. Since the MMO periodic orbit Γ_5 enters the attracting slow manifold in between canards ξ_4 and ξ_5, the number of small-amplitude oscillations is five. The MMO follows the repelling slow manifold S_ε^r for

a short while before it makes a large-amplitude excursion into the region of $v > 0$.

The curve labelled L^r in Figs. 1(b) and (c) represents one of the boundary conditions in our calculation of the canards and the repelling slow manifold S_ε^r. How these calculations are performed is explained next.

II. COMPUTING THE SLOW MANIFOLDS

Our numerical method is based on the idea that a part of interest of a two-dimensional manifold can be represented as a family of orbit segments. This family can be computed by continuation of the solutions of a suitable two-point boundary value problem, for example with the package AUTO [21, 22]. This general approach is quite powerful; see [23] for more examples of its use. The key is to set up and follow solutions to the right kind of boundary value problem.

To compute S_ε^a and S_ε^r we make use of the normal hyperbolicity of the critical manifold S [19]. Namely, for small $\varepsilon > 0$ the slow manifolds S_ε^a and S_ε^r are smooth perturbations of the critical manifold S, as long as one stays away from the fold curve F. In other words, sufficiently far away from F the surfaces S_ε^a and S_ε^r are approximated well by S, where the error goes to zero for $\varepsilon \to 0$. Therefore, we compute S_ε^a (and S_ε^r) as a one-parameter family of orbit segments of (2) where one end point varies along a curve on the critical manifold S that lies at a sufficient distance from F. To obtain a family of well-posed boundary value problems, the other end point is required to lie in a suitable plane transverse to the flow near F. As is explained below, this plane is chosen such that the resulting surface covers a particular region of interest.

A. Computation of the attracting slow manifold S_ε^a

As is common in the field of numerical continuation, we consider a vector field of the form

$$\dot{\mathbf{u}} = T\mathbf{g}(\mathbf{u}), \qquad (6)$$

where the (free) parameter T is the actual integration time. In other words, the total integration time of any solution of (6) is rescaled to 1. For the self-coupled FitzHugh Nagumo system $\mathbf{u} = (v, h, s)$ and $\mathbf{g}$ is the right-hand side of system (2). The idea is to continue solutions of system (6) subject to suitably chosen boundary conditions at $\mathbf{u}(0)$ and $\mathbf{u}(1)$, which can be achieved with numerical packages such as AUTO; see, for example, [5] for more background information on numerical continuation.

To ensure that solutions of (6) lie (in good approximation) on the attracting slow manifold S_ε^a we require that the begin point $\mathbf{u}(0)$ lies on a curve L^a on S that is sufficiently far away from F. Note that the best choice for $L^a \subset S$ would run 'parallel' to F, meaning that it lies at

an approximately uniformly large distance from F. Since S_ε^a is unbounded, L^a can be chosen as far from F as one wishes. In the computation of S_ε^a we used the boundary condition

$$\mathbf{u}(0) \in L^a := S \cap \{h = -6.0\}. \qquad (7)$$

To ensure that we compute the relevant part of S_ε^a near the folded node $\mathbf{p}_{\text{fn}}$, we restrict the end point $\mathbf{u}(1)$ to a plane Σ through $\mathbf{p}_{\text{fn}} \in F$ and transverse to the flow. A choice that works in general is to take the tangent vector of F at $\mathbf{p}_{\text{fn}}$ as the normal of Σ. However, only transversality is required and for system (2) a satisfactory choice is the plane of constant s, which gives the boundary condition

$$\mathbf{u}(1) \in \Sigma := \{(v, h, s) \in \mathbb{R}^3 \mid s = 0.2797\}. \qquad (8)$$

The solution family of the two-point boundary value problem (6)-(8), where the integration time T is a single free parameter, forms a good approximation of S_ε^a between L^a and Σ. We compute this solution family with the continuation and collocation routines of the package AUTO. A particular strength of AUTO is that the step length in the continuation is determined in terms of the L_2-norm between solutions. Therefore, the computed orbit segments are not only numerically accurate but also nicely spaced on the resulting surface, which is a distinct advantage for the rendering.

However, before S_ε^a can be computed one must first construct a solution of (6)-(8). To this end, we use a homotopy method with two steps. We first consider the family of orbit segment that solve (6) subject to (8) and the boundary condition

$$\mathbf{u}(0) \in F. \qquad (9)$$

Note that the trivial orbit segment given by the folded node, that is, $\{\mathbf{p}_{\text{fn}} \mid 0 \le t \le 1\}$, is a solution of (6) subject to (8) and (9) for $T = 0$. Starting from this trivial orbit, continuation in T grows the orbit where the endpoint is restricted to the fold curve F. This continuation is stopped when $\mathbf{u}(0)$ is at some predetermined distance from $\mathbf{p}_{\text{fn}}$, which is detected by a user-defined function in AUTO. Specifically, our computation was set to stop when

$$\mathbf{u}(0) \in \widetilde{\Sigma}^a := \{(v, h, s) \in \mathbb{R}^3 \mid s = 0.6\}. \qquad (10)$$

We then switch to the second step of the homotopy, which aims to move $\mathbf{u}(0) \in S$ away from F while remaining approximately at the same distance from Σ. Hence, we introduce the boundary condition

$$\mathbf{u}(0) \in \widetilde{L}^a = S \cap \widetilde{\Sigma}^a. \qquad (11)$$

and continue solutions of (6) subject to (8) and (11). The continuation is stopped when L^a is reached, which is again detected by a user-defined function in AUTO.

Figure 2(a) illustrates the continuations that are performed to obtain the first solution of (6)–(8). The dark
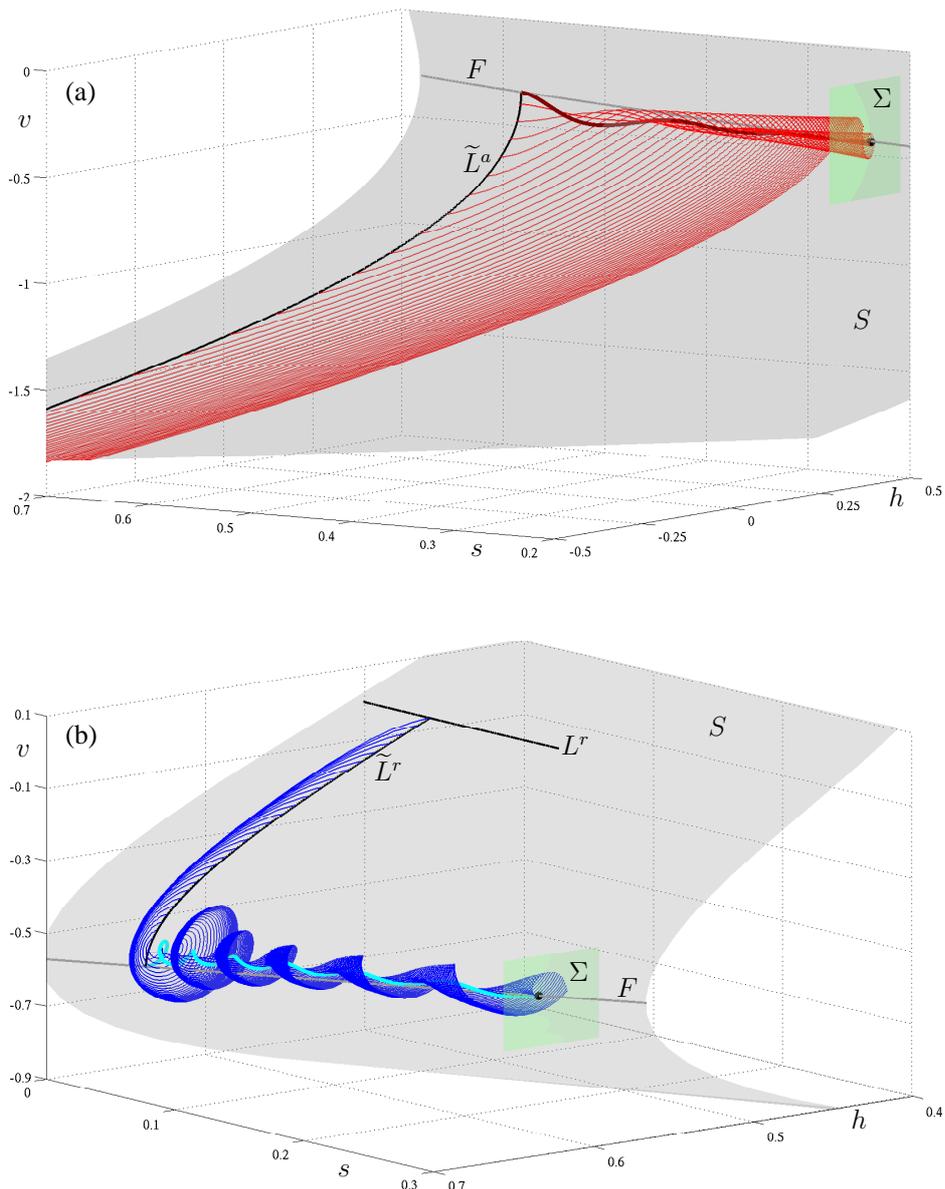
FIG. 2: Illustration of the homotopy steps needed to generate a suitable first orbit segment to start the computation of the attracting slow manifold S_ε^a (a) and the repelling slow manifold S_ε^r (b) of (2) for $\gamma = 0.5$, $\varepsilon = 0.015$, and $\delta = 0.565$; also shown are the critical manifold S and its fold curve F. The dark red orbit segment in panel (a) and the cyan orbit segment in panel (b) are obtained in the first homotopy step and connect $\widetilde{L}^a \cap F$ and $\widetilde{L}^r \cap F$, respectively, with the section Σ. The red and blue orbit segments are generated during the second homotopy step; the last of them is the sought-after first orbit segment from L^a and L^r, respectively, to the section Σ.

red curve is the orbit segment from $\widetilde{L}^a \cap F$ to the plane Σ as obtained at the end of the first homotopy step. This orbit is then continued while $\mathbf{u}(0)$ is restricted to $\widetilde{L}^a$ until $L^a = S \cap \{h = -6.0\}$ is reached. The red curves in Fig. 2(a) are a selection of orbit segments, shown near the fold curve F, that are computed during this second homotopy step. Note that these orbit segments do not form a good approximation of S_ε^a. However, as $\mathbf{u}(0)$ moves along $\widetilde{L}^a \subset S$ further away from F (in the direction of

decreasing h), the orbit segment $\{\mathbf{u}(t) \mid 0 \le t \le 1\}$ lies closer and closer to S_ε^a. The last of these orbits (with $\mathbf{u}(0) \in L^a$) is deemed close enough and serves as the start solution of the actual computation of S_ε^a from (6)-(8). The attracting slow manifold S_ε^a (red surface) in Fig. 1(c) was rendered from a total of 2700 orbit segments. Throughout the different steps we used a mesh of 400 mesh intervals (NTST = 100 and NCOL = 4) for each orbit segment.

B. Computation of the repelling slow manifold S_ε^r

The repelling slow manifold S_ε^r is computed in much the same way as S_ε^a. Namely, we consider negative T in (6), which effectively reverses the direction of the flow. However, there is an additional difficulty in that the repelling sheet of S is bounded by the fold curve. Therefore, the possibility of moving away from F by changing s is limited by the fact that one simultaneously approaches the other branch of F (with respect to the cusp point). This problem must be expected in general, namely it occurs for any system whose slow manifold is more complicated than a simple parabolic cylinder. Indeed the cusp surface considered here is a classic case. The best strategy is to restrict the begin point $\mathbf{u}(0)$ to a curve L^r that is 'furthest away' from the respective two bounding fold curves.

For the slow manifold S given by (3), one finds from (4) that the fold curve F is symmetric with respect to $v = 0$, so that the best choice for the boundary condition is

$$\mathbf{u}(0) \in L^r := S \cap \{v = 0.0\}. \tag{12}$$

The end point $\mathbf{u}(1)$ is again restricted to lie in the section Σ by imposing boundary condition (8). In other words, S_ε^r can be computed as the family of orbit segments that are solutions of (6) subject to (8) and (12).

As before, a first solution can be contructed in two homotopy steps. Namely, we again continue the boundary value problem (6) with boundary conditions (8) and (9) from the trivial orbit segment $\{\mathbf{p}_{\text{fn}} \mid 0 \le t \le 1\}$ with $T = 0$, but this time in the direction of negative T. We stop the continuation, when

$$\mathbf{u}(0) \in \widetilde{\Sigma}^r := \{(v, h, s) \in \mathbb{R}^3 \mid s = 0.05\} \tag{13}$$

as detected by a user-defined function in AUTO. We then switch to the second continuation run, where we solve system (6) subject to boundary conditions (8) and

$$\mathbf{u}(0) \in \widetilde{L}^r := S \cap \widetilde{\Sigma}^r. \tag{14}$$

The continuation now finds solution segments with $\mathbf{u}(0) \in \widetilde{L}^r$ that lie increasingly further away from F, and it stops when L^r is reached.

Figure 2(b) illustrates these continuations in the computation of S_ε^r. The cyan curve is the orbit segment from $\widetilde{L}^r \cap F$ to Σ, which is then continued in the second homotopy step while $\mathbf{u}(0)$ is restricted to $\widetilde{L}^r$ until $L^r = S \cap \{v = 0.0\}$ is reached. This continuation gives rise to the blue orbit segments in Fig. 2(b), the last of which is the start solution for the computation of S_ε^r with boundary conditions (8) and (12). The resulting image of the repelling slow manifold S_ε^r is shown in Fig. 1(c) (blue surface). As for S_ε^a, we used 400 mesh intervals for the 1200 orbit segments that make up the surface.
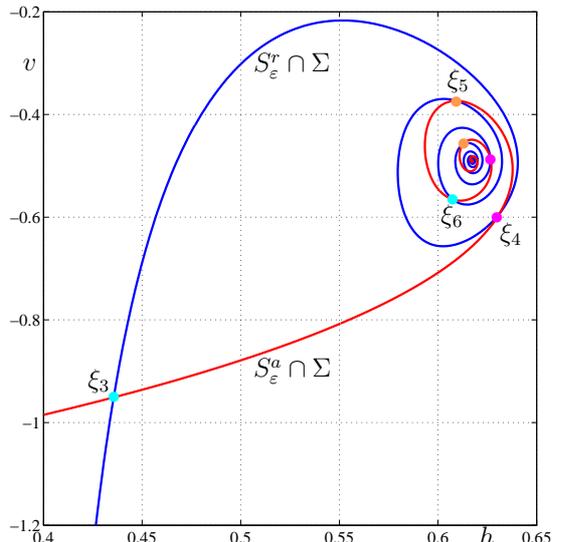

FIG. 3: The curves $S_\varepsilon^a \cap \Sigma$ and $S_\varepsilon^r \cap \Sigma$ in the plane Σ intersect at isolated points that correspond to the canard solutions of system (2). The image is for $\gamma = 0.5$, $\varepsilon = 0.015$, and $\delta = 0.565$ and the 'outermost' canard solutions ξ_3–ξ_8 are color coded as in Fig. 1.

C. Computation of canard solutions

The advantage of computing S_ε^a and S_ε^r up to the plane Σ, is that we can easily identify the canard solutions. Each (generic) canard solution ξ_i corresponds to an isolated intersection point of $S_\varepsilon^a \cap \Sigma$ and $S_\varepsilon^r \cap \Sigma$, as is illustrated in Fig. 3. The number of canard solutions can be determined in the normal form by the ratio of eigenvalues μ of the folded node $\mathbf{p}_{\text{fn}}$ [4, 6]; for the parameters of (2) as chosen $\mu \approx 55.5$, which means that we expect to find 29 canard solutions (2 primary canards and 27 secondary canards).

In our present setup, a canard solution is represented as a solution $\mathbf{u}$ of system (6) subject to the boundary conditions

$$\mathbf{u}(0) \in L^a \quad \text{and} \quad \mathbf{u}(1) \in L^r. \tag{15}$$

A solution of the boundary value problem (6) with (15) can be found as follows. We detect an orbit segment $\mathbf{u}^a$ on S_ε^a and an orbit segment $\mathbf{u}^r$ on S_ε^r that almost match up in the plane Σ, meaning that $\mathbf{u}^a(0) \approx \mathbf{u}^r(0) \in \Sigma$. From this pair of orbits we generate the concatenation of $\mathbf{u}^a$ with the reverse of $\mathbf{u}^r$ (which has positive rather than negative integration time). The resulting orbit segment is then rescaled back to the time interval $[0, 1]$, so that its integration time T is simply the sum of the two (now both positive) integration times for $\mathbf{u}^a$ and $\mathbf{u}^r$. Provided $|\mathbf{u}^a(0) - \mathbf{u}^r(0)|$ is sufficiently small, the application of a Newton step in AUTO generates a solution of (6) with (15) that represents the respective canard solution. The canard solution can then be continued in a system para-
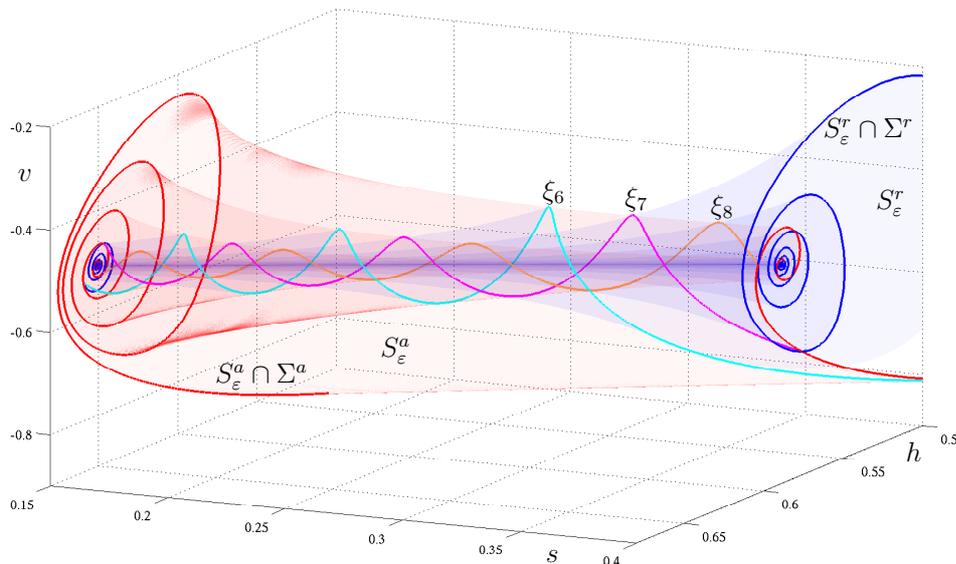
FIG. 4: The attracting slow manifold S^a_ε and the repelling slow manifold S^r_ε of system (2) for $\gamma = 0.5$, $\varepsilon = 0.015$, and $\delta = 0.565$, shown locally between the sections Σ^a of (17) and Σ^r of (18) with the three 'outermost' canard solutions ξ_6–ξ_8.

meter. In this way, it is possible to obtain information about how the canard solutions change with parameters; we refer to [6] for more details. Here we found the six canard solutions ξ_3–ξ_8 that are shown in Fig. 1(b). They were constructed by considering the respective intersection points of the curves $S^a_\varepsilon \cap \Sigma$ and $S^r_\varepsilon \cap \Sigma$ that are shown in Fig. 3. How selected canard solutions lie on S^a_ε and S^r_ε is illustrated in Fig. 1(c) and Fig. 4.

D. Visualizing the interaction of S^a_ε and S^r_ε

In Fig. 1 we computed S^a_ε and S^r_ε up to the plane Σ that contains the folded node $\mathbf{p}_{\text{fn}} \approx (-0.4900, 0.6176, 0.2797)$. Indeed, one can imagine that the dynamics in the silent-phase system (2) takes place on the attracting slow manifold S^a_ε before $\mathbf{p}_{\text{fn}}$ is reached, and on the repelling slow manifold S^r_ε from then on. However, to get a better idea of the geometry of the slow manifolds, in particular of how S^a_ε and S^r_ε intersect, both manifolds need to be computed past the plane Σ. This is straightforward in our boundary value problem setup.

Namely, we consider two new planes transverse to the flow close to the fold curve F. The most convenient choice for (2) is to take planes of the form

$$\Sigma_\sigma := \{(v, h, s) \in \mathbb{R}^3 \mid s = \sigma\}, \qquad (16)$$

which are parallel to $\Sigma = \Sigma_{0.2797}$. Specifically, we replace boundary condition (8) by

$$\mathbf{u}(1) \in \Sigma^a := \Sigma_{0.15} \qquad (17)$$

for the calculation of S^a_ε, and by

$$\mathbf{u}(1) \in \Sigma^r := \Sigma_{0.40}. \qquad (18)$$

for the calculation of S^r_ε.

A start solution on S^a_ε that satisfies (17) can be obtained from an orbit segment $\mathbf{u}$ from L^a to Σ by continuation in T and the parameter σ of the section Σ_σ, where we start from $\sigma = 0.2797$. Here we keep $\mathbf{u}(0)$ fixed and require that $\mathbf{u}(1) \in \Sigma^a$. This continuation is stopped when Σ^a is reached, which is detected by a user-defined function in AUTO. Similarly, an orbit segment on S^r_ε can be continued up to Σ^r to obtain a start solution that satisfies (18).

The computation of S^a_ε and S^r_ε can now be performed as before. The two slow manifolds are shown in Fig. 4, where we clipped the surfaces so that only the part in between Σ^r and Σ^a is visualised. This kind of representation is designed to give good geometric insight into how the two manifolds intersect near $\mathbf{p}_{\text{fn}}$ and give rise to canard solutions. The three canard solutions ξ_6, ξ_7 and ξ_8 are shown in Fig. 4.

The silent-phase system (2) and, hence, the geometry of its slow manifolds, does not depend on the activation rate β. Rather, β controls the relaxation oscillation during the active phase and, in particular, where exactly the orbit returns back to the silent phase. As a result, varying β causes the resulting MMO to move relative to the canard solutions on S^a_ε, which means that the number of small oscillations can be adjusted by changing β.

This phenomenon is illustrated in Fig. 5, where we show the computed slow manifolds S^a_ε and S^r_ε of system (2) subject to boundary conditions (17) and (18), together with the canard solutions ξ_5–ξ_7. Also shown are the two MMO periodic orbits Γ_6 and Γ_7 of type 1^6 and 1^7 of system (1) for $\beta = 0.043$ and $\beta = 0.048$, respectively. Figure 5(c) clearly shows how the MMO Γ_k enters the attracting slow manifold (after the excursion
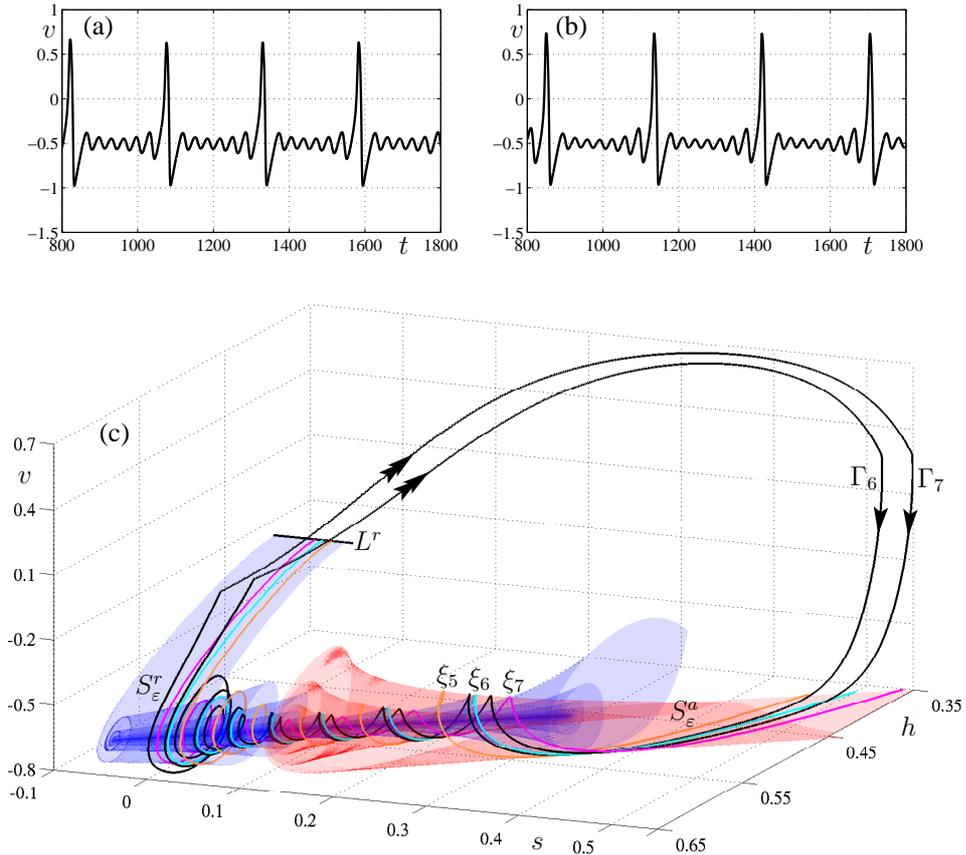
FIG. 5: A larger view of the slow manifolds S_ε^a and S_ε^r of Fig. 4 and the canard solutions ξ_5–ξ_7. Panels (a) and (b) show the MMOs of system (1) for $\beta = 0.043$ and $\beta = 0.048$, respectively. Panel (c) shows the corresponding MMO periodic orbits Γ_6 and Γ_7 relative to S_ε^a, S_ε^r and the canard solutions ξ_5–ξ_7; compare also with Fig. 1.

corresponding to the active phase) in between the canard orbits ξ_{k-1} and ξ_k, and the orbit stays in this region during the whole silent phase. This geometry explains the different types of MMOs and their dependance on β in the self-coupled FitzHugh Nagumo system (1).

III. DISCUSSION

We presented the technique of computing slow manifolds and corresponding canard solutions in slow-fast systems by means of solving suitable two-point boundary value problems. Specifically, two-dimensional attracting and repelling slow manifolds can be found in this way as a family of orbit segments starting on a curve on the critical manifold and ending in a prescribed section. We showed how an inititial solution of this sort can be generated by specified continuation runs. We used the package AUTO [21, 22] for solving the BVPs, that is, their solutions are found with the method of collocation as piecewise polynomials on a defined mesh. This provides global accuracy along orbit segments, which is a distinct advantage over shooting methods in the context of slow-fast systems.

We illustrated the methods with the example of the self-coupled FitzHugh Nagumo system. We considered the geometry of the slow manifold as given by the silent-phase system. It is governed by a folded node singularity that gives rise to canard solutions and we brought out this dynamics by computing the attracting and repelling slow manifolds. These manifolds are divided by the canard solutions into regions corresponding to different types of MMOs when they are subject to the active phase of the system.

Overall, we demonstrated how the calculation of the slow manifolds of the self-coupled FitzHugh Nagumo system can lead to geometrical insight into the dynamics of a slow-fast system arising in an application. A more detailed bifurcation study of canard solutions remains an interesting topic beyond the scope of this paper. In the future we plan to apply this technique also to other slow-fast models with two-dimensional slow manifolds. Indeed there are many such examples, including models of neuron [3, 24] and chemical [2, 20, 25] systems.

[1] V. Petrov, S. K. Scott, and K. Showalter, J. Chem. Phys. **97**, 6191 (1992).

[2] A. Milik, P. Szmolyan, H. Löffelmann, and E. Gröller, Internat. J. Bifur. Chaos Appl. Sci. Engrg. **8**, 505 (1998).

[3] J. Rubin and M. Wechselberger, Biological Cybernetics **97**, 5 (2007).

[4] M. Wechselberger, SIAM J. Appl. Dyn. Sys. **4**, 101 (2005).

[5] B. Krauskopf, H. M. Osinga, and J. Galán-Vioque, *Numerical Continuation Methods for Dynamical Systems: Path following and boundary value problems* (Springer-Verlag, New-York, 2007).

[6] M. Desroches, B. Krauskopf, and H. M. Osinga (2007), preprint.

[7] J. Guckenheimer (2007), preprint.

[8] E. Benoît, in *Troisième rencontre du Schnepfenried* (Soc. Math. France, 1983), vol. **109–110** of *Astérisque*, pp. 159–191.

[9] W. Eckhaus, *Asymptotic Analysis II* (Springer-Verlag, New-York, 1983), vol. **958** of *Lecture Notes in Math.*, chap. Relaxation oscillations including a standard chase on French ducks, pp. 449–494.

[10] R. Roussarie, in *Bifurcations and Periodic Orbits of Vector Fields*, edited by D. Szlomiuk (Kluwer Academic, Dordrecht, 1993), pp. 347–382.

[11] C. K. R. T. Jones, *Dynamical Systems, C.I.M.E Lectures, Montecatini Terme, June 1994* (Springer-Verlag, New-York, 1995), vol. **1609** of *Lecture Notes in Math.*, chap. Geometric singular perturbation theory, pp. 44–120.

[12] F. Dumortier and R. Roussarie, Mem. Amer. Math. Soc. **121** (1996).

[13] P. Szmolyan and M. Wechselberger, J. Differential Equations **177**, 419 (2001).

[14] P. Szmolyan and M. Wechselberger, J. Differential Equations **200**, 69 (2004).

[15] J. Guckenheimer, K. A. Hoffman, and W. Weckesser, SIAM J. Appl. Dyn. Sys. **2**, 1 (2003).

[16] K. Bold, C. Edwards, J. Guckenheimer, S. Guharay, K. Hoffman, J. Hubbard, R. Oliva, and W. Weckesser, SIAM J. Appl. Dyn. Sys. **2**, 570 (2003).

[17] J. Guckenheimer and R. Haiduc, Mosc. Math. J. **5**, 91 (2005).

[18] M. Brøns, M. Krupa, and M. Wechselberger, in *Fields Institute Communications* (Amer. Math. Soc., Providence, RI, 2006), vol. **49**, pp. 39–63.

[19] N. Fenichel, J. Differential Equations **31**, 53 (1979).

[20] M. T. M. Koper, Physica D **80**, 72 (1995).

[21] E. J. Doedel, Congr. Numer. **30**, 265 (1981).

[22] E. J. Doedel, R. C. Paffenroth, A. R. Champneys, T. F. Fairgrieve, Y. A. Kuznetsov, B. E. Oldeman, B. Sandstede, and X. J. Wang, available via `http://cmvl.cs.concordia.ca/`.

[23] B. Krauskopf and H. M. Osinga, in *Numerical Continuation Methods for Dynamical Systems: Path following and boundary value problems*, edited by B. Krauskopf, H. M. Osinga, and J. Galán-Vioque (Springer-Verlag, New-York, 2007), pp. 117–154.

[24] J. Rubin and D. Terman, in *Handbook of Dynamical Systems*, edited by B. Fiedler (Noth-Holland, Amsterdam, 2002), vol. 2, pp. 93–146.

[25] J. Moehlis, J. Nonlin. Sci. **12**, 319 (2002).